*International Geology Review*, Vol. 49, 2007, p. 732–752.


# Petrology and U-Pb SHRIMP Geochronology of a Garnet Peridotite, Sulu UHP Terrane, East-Central China

RUIXUAN ZHAO, JUHN G. LIOU,[1] TATSUKI TSUJIMORI,[2] AND RU Y. ZHANG

*Department of Geological and Environmental Sciences, Stanford University, Stanford, California 94305-2115*

## Abstract

Garnet clinopyroxenite at Rizhao occurs as a lens 100 × 225 $m^2$ within a serpentinized peridotite body, in fault contact with felsic gneiss. Minor dunite also occurs within the same peridotite. The clinopyroxenite consists of porphyroblastic Grt-bearing (type 1), megacrystic Grt-bearing (type 2), porphyroblastic Cpx-bearing (type 3), and equigranular (type 4) garnet clinopyroxenite. Lamellae-rich, coarse-grained Cpx occurs as inclusions in megacrystic Grt from type 2 clinopyroxenite, and as porphyroblasts in a matrix of Cpx + Grt + Ilm from type 3 clinopyroxenite; these clinopyroxenes contain abundant exsolution lamellae of Grt ($Prp_{16\text{-}19}Grs_{62}Alm_{19\text{-}21}Sps_1$) + Ilm ± Mag ± Amp (Mg#: 0.88–0.98; $Na_2O$: 0.5–3.3 wt%; $K_2O$: 0.7–1.0 wt%; $TiO_2$: 0.1–0.2 wt%). Megacrystic and porphyroblastic garnet ($Prp_{35\text{-}42}Grs_{34\text{-}45}Alm_{19\text{-}24}Sps_1$) also occurs in a matrix of fine-grained Cpx + Grt + Ilm; spinel (Mg#: 0.60–0.62) is present as inclusions in both porphyroblastic Grt and lamellae-rich Cpx. Petrochemical data support a mantle origin involving crystallization of majoritic garnet. We propose that the protolith of the Rizhao clinopyroxenite initially was a spinel clinopyroxenite, and was convected to great depths (>450 km) to form a majoritic garnet that contains high CaO and considerable amounts of FeO and $TiO_2$. During later decompression, the majoritic garnet broke down to form intergrowths of Cpx + Grt + Ilm ± Mag ± Amp at T = 700–800°C, P ≤ 3 GPa. It was then emplaced into a subduction zone and experienced UHP metamorphism at 620–880°C, 3 GPa during Triassic continental collision. Megacrystic/porphyroblastic garnet formed during this stage, and lamellae-rich Cpx recrystallized to the matrix assemblage of Cpx + Grt + Ilm subsequently. The clinopyroxenite also experienced later retrogression during exhumation. Zircon U-Pb geochronology yields 215 ± 2 Ma for the Rizhao garnet clinopyroxenite; occurrence of garnet and clinopyroxene inclusions in zircon suggests that this age reflects the UHP metamorphism.



## Introduction

GARNET PERIDOTITES are volumetrically small but widespread in ultrahigh-pressure (UHP) metamorphic terranes in continental collision zones. Garnet peridotites constitute an important petrological component of UHP terranes and are regarded as a window to upper mantle processes. They carry important geodynamic implications for continental collision, provide information on crust-mantle interaction and emplacement of mantle rocks into continental crust during continental collision, and are an important source of information on the composition and evolution of the local upper mantle. It has been suggested that HP/UHP peridotites show different initial tectonic settings, evolutionary histories, and emplacement mechanisms not only in different orogens, but also within an individual terrane (Medaris, 1999; Brueckner and Medaris, 1998, 2000; Zhang et al., 2000). Garnet peridotites from the Dabie-Sulu terrane have been subdivided into Type A peridotites that are upper mantle slivers emplaced into the subducted slab at mantle depths, and Type B peridotites that resided in the continental crust prior to the subduction (Zhang et al., 2000). Both types were subjected to UHP metamorphism during continental collision. However, the initial tectonic setting and evolution may vary from locality to locality, and it is not straightforward to identify their origin because of their complex metamorphic histories. For example, the association with metagabbro and metagranite favors a crustal intrusion origin for the Yangkou ultramafic complex; petrochemical and O-isotope data suggest a mantle origin (Zhang et al., 2005b). These authors suggested that further age data are needed to determine if the ultramafic complex had

[1]Corresponding author; email: liou@pangea.stanford.edu

[2]Present address: The Pheasant Memorial Laboratory for Geochemistry and Cosmochemistry, Institute for Study of the Earth's Interior, Okayama University, Misasa, Tottori 682-0193, Japan.

an identical protolith age as the mafic rocks, and thus would give a better interpretation of its origin.

Geochronology in addition to petrological and geochemical investigations is important. It will answer important questions such as identifying the protolith age of the garnet peridotites, and determining whether or not they were subjected to *in situ* UHP metamorphism together with the surrounding country rocks. Combined with petrochemistry, it will also help to solve problems regarding the origin of these garnet peridotites, the mechanism for their emplacement into the subduction zone, and their pressure-temperature-time paths. To date, only a few SHRIMP zircon dates are available for garnet peridotites (Rumble et al., 2002; Yang et al., 2003; Zhang et al., 2005c; Zhao et al., 2006) because of the lack of zircons in these rocks. Most geochronological studies have been done by the Sm-Nd isochron method, which in some cases produces meaningless ages because of isotopic disequilibrium (Yang and Jahn, 2000). In this paper, a new SHRIMP U-Pb zircon age is determined in addition to a detailed petrological study of the Rizhao peridotites from the Sulu terrane. Their metamorphic evolution history, peak P-T conditions, and timing of UHP metamorphism will also be discussed.

## Geological Settings

The Qinling-Dabie-Sulu collision zone lies between the Sino-Korean and Yangtze cratons. The Sulu terrane is the eastern extension of the Qinling-Dabie belt, and has been displaced northward by the sinistral Tan-Lu fault. The Sulu UHP terrane is bounded by the Yantai-Qingdao-Wulian (WQYF) fault on the northwest and the Jiashan-Xiangshui (JXF) fault on the south (Fig. 1A). The Sulu terrane consists of two fault-bounded UHP and HP belts, intruded by post-orogenic Cretaceous granite. The UHP belt consists mainly of amphibolite- to granulite-facies orthogneiss, paragneiss, amphibolite, and minor marble. Meter- to kilometer-sized metamorphosed garnet peridotite and pyroxenite are widespread, and occur sporadically as blocks and thin layers in the gneiss (Zhang and Liou, 1998). Coesite-bearing eclogite bodies also occur as lenses and layers in the gneiss; the remainders are enclosed as pods in ultramafic rocks and in marble. Coesite is preserved as inclusions in zircon from many country-rock gneisses, confirming the *in situ* UHP metamorphism of the Sulu region (Ye et al., 2000; Liu et al., 2002). The HP belt, southeast of the UHP belt, consists mainly of quartz-mica schist, chloritoid-kyanite-mica-quartz schist, marble, and rare blueschist (Zhang et al., 1995).

The Hujialing ultramafic complex in Rizhao in the mid-south of the Sulu terrane is one of the largest ultramafic bodies in the Dabie-Sulu UHP terrane (Fig. 1B). The ultramafic body (0.2–1 × 2 $km^2$ in size) is faulted against gneiss. It consists mainly of serpentinized peridotite, containing discontinuous lenses of garnet clinopyroxenite, garnet olivine clinopyroxenite and dunite surrounded by serpentinite at its margins (Fig. 1C). To the east of the studied body, clinopyroxenite, olivine-bearing clinopyroxenite, serpentinite, and eclogite crop out; inclusions of quartz pseudomorphs after coesite and exsolved rutile needles are preserved in eclogitic garnet (Zhang and Liou, 2003). Zhang and Liou (2003) studied two representative garnet clinopyroxenites with exsolution microstructures from the Hujialing peridotite body: (1) an ilmenite-rich sample composed of coarse-grained clinopyroxene containing abundant exsolutions of garnet + ilmenite; and (2) a megacrystic garnet-bearing sample with exsolution-rich clinopyroxene inclusions in garnet. They proposed that the parental phase of exsolved garnet + ilmenite exsolutions and clinopyroxene host was either a homogeneous clinopyroxene formed at near-solidus conditions (≤1400°C, at 5 GPa) in the upper mantle, or a majoritic garnet from the mantle transition zone (>450 km depth). These two hypotheses remain to be tested.

## Petrography

### *Garnet clinopyroxenite*

Samples were collected from the largest garnet pyroxenite lens (Fig. 1D), which is 100 × 225 m in size, and nearby outcrops. This lens mainly consists of porphyroblastic garnet clinopyroxenite with or without olivine (type 1), megacrystic garnet-bearing clinopyroxenite (type 2), porphyroblastic clinopyroxene-bearing garnet clinopyroxenite (type 3), and equigranular garnet clinopyroxenite (type 4). Most garnet clinopyroxenites belong to type 1 or 4; only a few contain coarse-grained clinopyroxenes with abundant exsolution (type 3). One garnet clinopyroxenite layer in the central part of the lens contains ellipsoidal to spherical garnet megacrysts up to 12 cm across (type 2).

*Type 1. Porphyroblastic garnet-bearing clinopyroxenite (2G, 2F, 15A, 23A).* Type 1 clinopyroxenite consists mainly of porphyroblastic garnet in a matrix

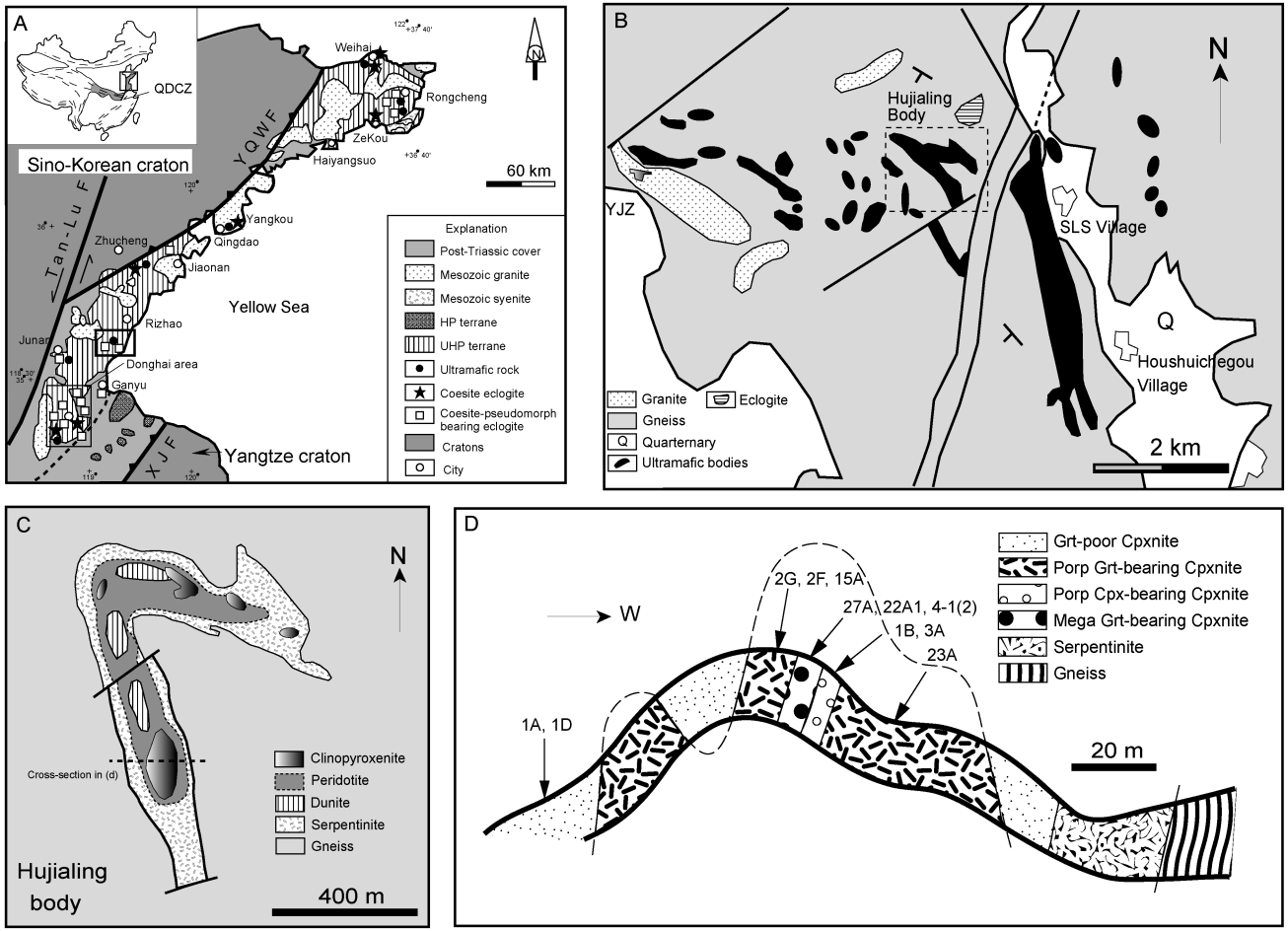


FIG. 1. A. Simplified geological map of the Sulu terrane, east-central China, showing localities of garnet peridotite and eclogite in the UHP unit. B and C. Geological sketch map of the Rizhao area showing localities of the Hujialing ultramafic body. D. Simplified cross-section showing localities of investigated samples (modified after Zhang et al., 1994; Zhang and Liou, 2003).

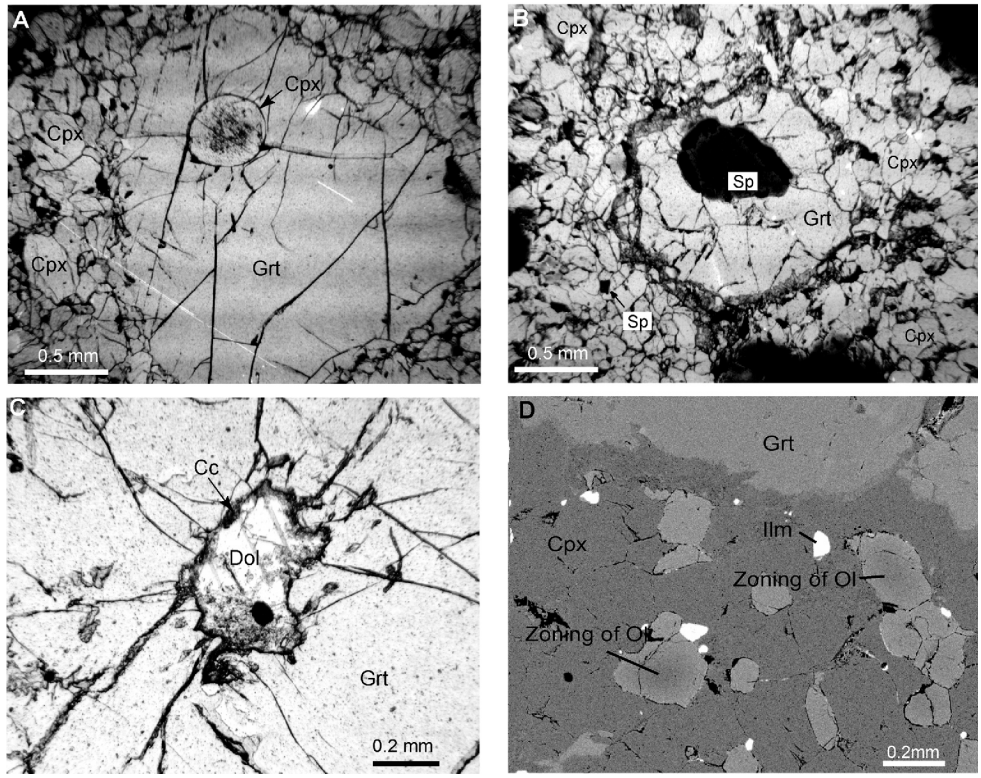


FIG. 2. A–C. Photomicrographs showing a lamellae-rich clinopyroxene (Cpx) inclusion (A), a spinel (Spl) inclusion (B), and a dolomite (Dol) inclusion (C) in porphyroblastic garnets (Grt) from the Rizhao garnet clinopyroxenite. All photos are plane-polarized light. D. BSE image of zoned olivines from the Rizhao garnet clinopyroxenite.



of Grt, Cpx, Ilm, and Spl. Garnets occur as both porphyroblasts (2 to 4 mm in size) and a fine-grained matrix (<0.5 mm in size). Coarse-grained garnets contain exsolution-rich Cpx (Fig. 2A) and green Spl inclusions (Fig. 2B). A coarse-grained garnet also contains a dolomite inclusion in sample 23A; dolomite is replaced by calcite at the rim (Fig. 2C). Fine-grained clinopyroxene (0.1–0.4 mm in size) occurs in the matrix together with ilmenite, magnetite, and green spinel. In sample 2G, zoned olivine (0.2–0.4 mm) occurs in the matrix (Fig. 2D).

*Type 2. Megacrystic garnet-bearing clinopyroxenite (27A, 22A1, 3A-1, 4-1).* Megacrystic garnet-bearing clinopyroxenite consists of variable amounts of megacrystic garnets (2.5–12 cm in diameter) in a fine-grained matrix of Grt + Cpx + Ilm (0.2–0.4 mm). Abundant coarse-grained inclusions of clinopyroxene and ilmenite (+ minor spinel and amphibole) are preserved in the megacrystic garnet. The clinopyroxene inclusions contain abundant exsolutions including garnet rods or blebs and oriented amphibole and ilmenite lamellae, which are confined in the core of Cpx (Fig. 3). Garnet blebs make up from 1 to 15 vol% of the clinopyroxene host. The amphibole lamellae are 0.01–0.04 mm wide and 0.4–0.6 mm long. Short rods of ilmenite (0.01–0.02 mm wide and 0.05–0.3 mm long) are oriented nearly perpendicular to the amphibole lamellae. In sample 4-1, amphibole also occurs as primary inclusions and as a rim around the clinopyroxene inclusion in the megacrystic garnet; a secondary vein consisting of Amp + Chl + Ep + Spl aggregates also crosscuts garnet megacrysts. In sample 22A1, megacrystic garnet has been completely replaced by secondary minerals (plagioclase, epidote, chlorite), whereas cpx inclusions are still preserved and contain garnet inclusions and few ilmenite rods (Fig. 4A).

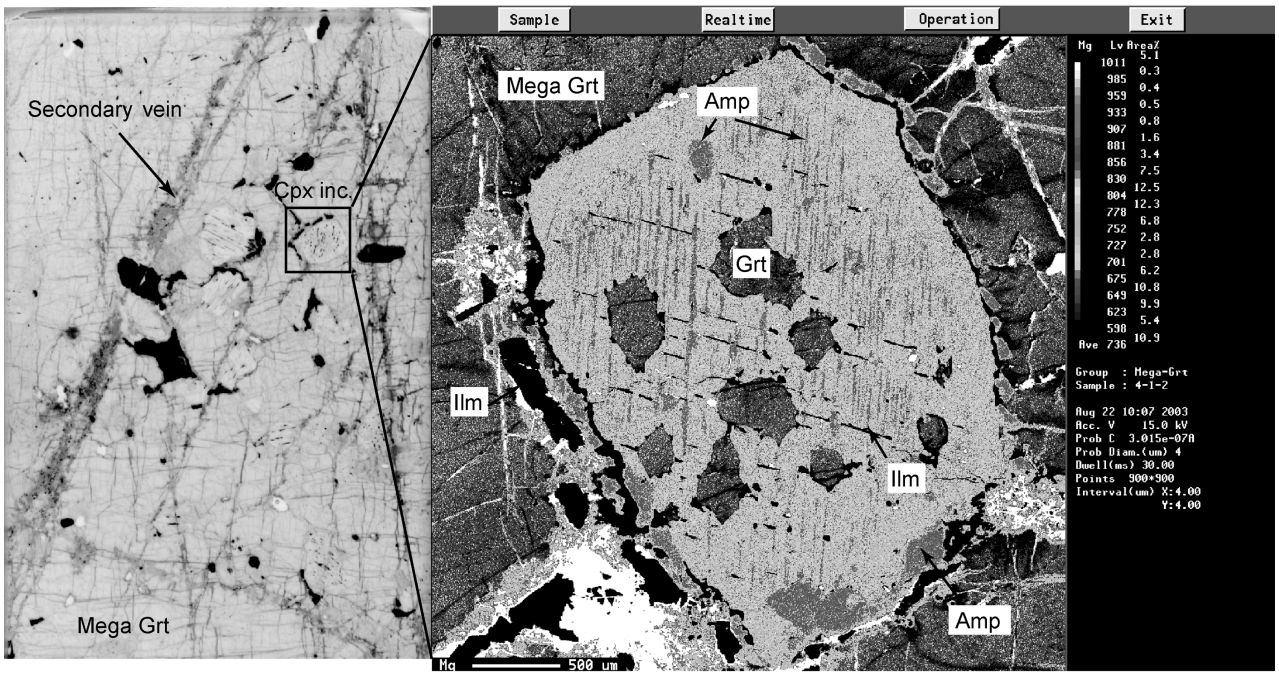


FIG. 3. A. Photomicrograph showing lamellae-rich clinopyroxene (Cpx) inclusions in a megacrystic garnet (Grt). B. X-ray image of Mg (Kα) for clinopyroxene inclusion containing abundant garnet (Grt) blebs, amphibole (Amp), and ilmenite (Ilm) exsolution lamellae.

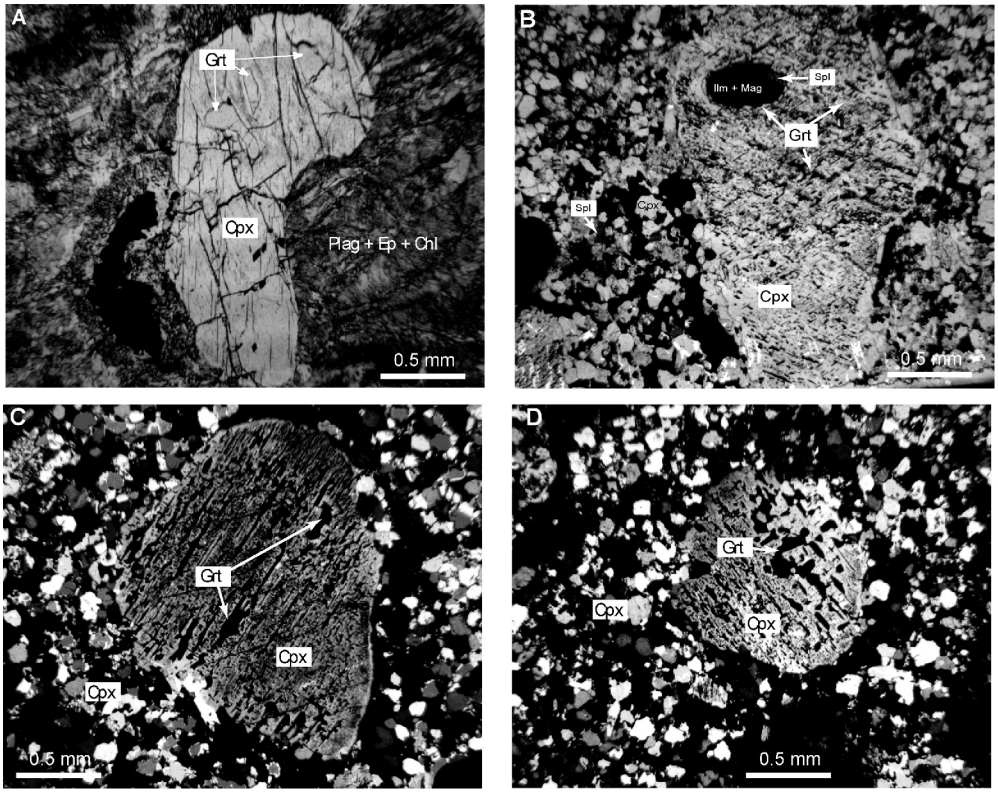


FIG. 4. A. Photomicrograph showing a lamellae-bearing clinopyroxene (Cpx) inclusion in a megacrystic garnet (Grt), which has been completely replaced by secondary plagioclase, epidote, and chlorite (Plag + Ep + Chl). B. Lamellae-rich clinopyroxene porphyroblast contains spinel + ilmenite + magnetite inclusion, which is surrounded by a thin garnet rim. C and D. Photomicrographs showing lamellae-rich clinopyroxene porphyroblasts in a matrix of fine-grained Cpx + Grt + Ilm. A and B are plane-polarized light; C and D are crossed-polars.



*Type 3. Porphyroblastic clinopyroxene-bearing clinopyroxenite (1B, 3A).* Porphyroblastic clinopyroxene-bearing clinopyroxenite contains coarse-grained clinopyroxene (0.8–4 mm) with abundant garnet, ilmenite, and magnetite exsolution lamellae (Fig. 5). The fine-grained matrix (0.1–0.3 mm) consists of Cpx + Ilm with minor Grt, Spl, and Mag (Figs. 4B, 4C, and 4D). Garnet exsolution occurs as relatively large elongated blebs (0.2 × 0.03 mm), whereas Ilm ± Mag occur as small lamellae (0.05 mm long) in the host clinopyroxene. Magnetite typically occurs as smaller, isolated rods or intergrowths with ilmenite, and appears to be exsolved from early-formed ilmenite (Fig. 5). Minor garnet and green spinel also occur in the matrix. In sample 3A, an intergrown Spl + Ilm + Mag inclusion occurs in a porphyroblastic clinopyroxene; a thin garnet rim grows around the inclusion (Fig. 4B). Parallel layers consisting of fine-grained Ilm also exist in the matrix of this sample. Although ilmenite grains do not show elongated shapes caused by deformation, pressure shadows consisting of ilmenite are present around the clinopyroxene porphyroblasts.

*Type 4. Equigranular garnet clinopyroxenite (1A, 1D).* This type of garnet clinopyroxenite is equigranular and composed of Grt + Cpx + Ilm. Garnets (0.2–0.4 mm) occur as interstitial phases between clinopyroxenes (0.1–0.3 mm). Some garnet grains are surrounded by a thin kelyphitic corona of epidote, plagioclase, and chlorite.

### *Dunite*

Dunite crops out along the margin of the clinopyroxenite body, and consists of >90 vol% equigranular olivine (0.2–0.3 mm in size). Chromite occurs as interstitial grains between olivine grains. Minor

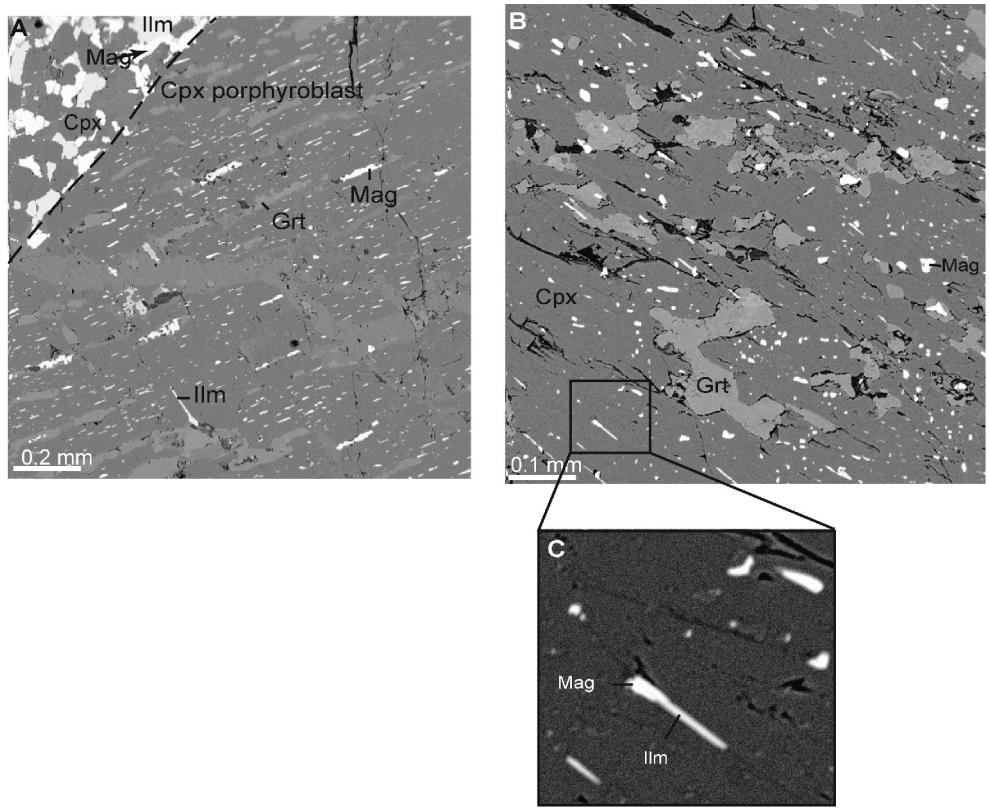


FIG. 5. A and B. BSE images showing garnet (Grt), ilmenite (Ilm), and magnetite (Mag) exsolutions in host clinopyroxenes (Cpx). C. BSE images showing ilmenite and magnetite intergrowths in clinopyroxene.

secondary amphibole, talc, and chlorite are also present.

## Mineral Chemistry

Mineral compositions of representative garnet clinopyroxenite (2G, 2F, 15A, 1B, 3A, 27A, 4-1) and dunite (3B) were analyzed employing a JEOL superprobe 733 at Stanford University under the operating conditions 15kv acceleration potential, 12 nA beam current, and peak counting times of 20 seconds. Total iron is expressed as FeO. All Fe is assumed to be $Fe^{2+}$ for olivine, garnet, and clinopyroxene. The $Fe^{3+}$ content of chromite was calculated from charge balance, assuming total cations = 3. The results are described as follows (see Table 1).

### *Garnet*

Compositions of analyzed garnets are plotted in Figure 6A. For porphyroblastic or megacrystic garnet-bearing clinopyroxenites (type 1 and 2), garnet has a similar composition regardless whether it occurs as in porphyroblast, megacryst, or matrix. For sample 15A, porphroblastic garnets that contain green spinel have an average composition of $Prp_{35.8}Grs_{41}Alm_{22.7}Sps_{0.5}$, whereas the composition of garnets in the matrix is lower in pyrope, but higher in grossular content (about $Prp_{30.7}Grs_{47.8}Alm_{21.1}Sps_{0.4}$). For sample 27A, the megacrystic garnet is homogeneous in composition with $Prp_{34.9}Grs_{45.4}Alm_{19.4}Sps_{0.3}$ on average, which is slightly higher in grossular and lower in almandine content than that from porphyroblastic garnet; garnet in matrix has an average composition of $Prp_{32.4}Grs_{48.3}Alm_{19}Sps_{0.3}$. For sample 2G, porphyroblastic and matrix garnet has an average composition of $Prp_{36.1}Grs_{40.1}Alm_{23.2}Sps_{0.6}$. For sample 2F, porphyroblastic garnet has an average composition of $Prp_{41.6}Grs_{34.1}Alm_{23.7}Sps_{0.6}$, whereas the matrix garnet has an average composition of

TABLE 1. Representative Mineral Analyses of the Rizhao Dunite and Garnet Clinopyroxenite

| | Dunite 3B | | Clinopyroxenite 2G | | | | Clinopyroxenite 2F | | | Clinopyroxenite 15A | | | |
|---|---|---|---|---|---|---|---|---|---|---|---|---|---|
| Mineral | Ol | Spl | Ol (matrix) | Grt (matrix) | Cpx (matrix) | Spl (matrix) | Grt (porp) | Grt (matrix) | Cpx (matrix) | Grt (porp) | Grt (matrix) | Cpx (matrix) | Spl (inc) |
| $SiO_2$ | 40.88 | 0.00 | 39.46 | 40.18 | 55.60 | 0.04 | 40.83 | 40.39 | 55.16 | 40.31 | 40.74 | 55.64 | 0.00 |
| $TiO_2$ | 0.00 | 0.00 | 0.00 | 0.05 | 0.02 | 0.04 | 0.08 | 0.05 | 0.00 | 0.06 | 0.04 | 0.00 | 0.00 |
| $Cr_2O_3$ | 0.00 | 53. 15 | 0.00 | 0.34 | 0.01 | 2.34 | 0.38 | 0.51 | 0.10 | 0.30 | 0.19 | 0.00 | 4.94 |
| $Al_2O_3$ | 0.00 | 9.31 | 0.00 | 21.52 | 0.75 | 61.57 | 21.60 | 21.26 | 0.72 | 21.66 | 21.77 | 0.93 | 57.75 |
| FeO | 7.85 | 29.05 | 16.69 | 11.91 | 1.47 | 23.06 | 11.24 | 11.69 | 1.67 | 10.86 | 10.46 | 1.75 | 20.74 |
| MnO | 0.04 | 0.45 | 0.15 | 0.37 | 0.00 | 0.14 | 0.30 | 0.23 | 0.05 | 0.19 | 0.19 | 0.00 | 0.04 |
| MgO | 51.25 | 5.12 | 43.03 | 9.32 | 17.02 | 13.90 | 11.26 | 9.12 | 17.16 | 9.45 | 8.78 | 17.02 | 15.48 |
| CaO | 0.00 | 0.00 | 0.00 | 15.83 | 25.22 | 0.17 | 13.19 | 16.07 | 23.73 | 16.53 | 17.81 | 24.83 | 0.00 |
| $Na_2O$ | 0.00 | 0.00 | 0.00 | 0.00 | 0.53 | 0.00 | 0.01 | 0.00 | 0.58 | 0.00 | 0.00 | 0.38 | 0.00 |
| Total | 100.01 | 97.43 | 99.34 | 99.51 | 100.62 | 101.25 | 98.89 | 99.33 | 99.17 | 99.35 | 99.98 | 100.57 | 98.96 |
| Si | 0.99 | 0.00 | 1.00 | 3.01 | 2.00 | 0.00 | 3.04 | 3.03 | 2.01 | 3.02 | 3.03 | 2.00 | 0.00 |
| Ti | 0.00 | 0.00 | 0.00 | 0.00 | 0.00 | 0.00 | 0.00 | 0.00 | 0.00 | 0.00 | 0.00 | 0.00 | 0.00 |
| Cr | 0.00 | 1.51 | 0.00 | 0.02 | 0.00 | 0.05 | 0.02 | 0.03 | 0.00 | 0.02 | 0.01 | 0.00 | 0.11 |
| Al | 0.00 | 0.39 | 0.00 | 1.90 | 0.03 | 1.91 | 1.90 | 1.88 | 0.03 | 1.91 | 1.91 | 0.04 | 1.83 |
| $Fe^{3+}$ | | 0.10 | | | | 0.04 | | | | | | | 0.06 |
| $Fe^{2+}$ | 0.16 | 0.76 | 0.36 | 0.75 | 0.04 | 0.46 | 0.70 | 0.73 | 0.05 | 0.68 | 0.65 | 0.05 | 0.41 |
| Mn | 0.00 | 0.01 | 0.00 | 0.02 | 0.00 | 0.00 | 0.02 | 0.01 | 0.00 | 0.01 | 0.01 | 0.00 | 0.00 |
| Mg | 1.85 | 0.27 | 1.63 | 1.04 | 0.91 | 0.54 | 1.25 | 1.02 | 0.93 | 1.05 | 0.97 | 0.91 | 0.62 |
| Ca | 0.00 | 0.00 | 0.00 | 1.27 | 0.97 | 0.00 | 1.05 | 1.29 | 0.93 | 1.32 | 1.42 | 0.96 | 0.00 |
| Na | 0.00 | 0.00 | 0.00 | 0.00 | 0.04 | 0.00 | 0.00 | 0.00 | 0.04 | 0.00 | 0.00 | 0.03 | 0.00 |
| Total | 7.01 | 7.05 | 3.00 | 8.02 | 4.00 | 3.02 | 7.99 | 8.01 | 3.99 | 8.02 | 8.01 | 3.99 | 3.03 |

*Table continues*

TABLE 1. *Continued*

| | Clinopyroxenite 1B | | | Clinopyroxenite 3A | | | | | Clinopyroxenite 27A | | | |
|---|---|---|---|---|---|---|---|---|---|---|---|---|
| Mineral | Grt (exs) | Cpx (porp) | Cpx (matrix) | Grt (matrix) | Grt (exs) | Cpx (matrix) | Cpx (porp) | Spl (inc in Cpx) | Grt (mega) | Grt (matrix) | Cpx (inc in mega Grt) | Cpx (matrix) |
| $SiO_2$ | 40.05 | 54.43 | 54.50 | 39.25 | 40.21 | 56.53 | 55.99 | 0.00 | 41.12 | 41.05 | 56.35 | 56.36 |
| $TiO_2$ | 0.19 | 0.15 | 0.06 | 0.39 | 0.27 | 0.00 | 0.07 | 0.00 | 0.12 | 0.04 | 0.02 | 0.00 |
| $Cr_2O_3$ | 0.02 | 0.01 | 0.03 | 0.00 | 0.00 | 0.00 | 0.00 | 0.00 | 0.05 | 0.15 | 0.00 | 0.00 |
| $Al_2O_3$ | 20.78 | 2.30 | 1.39 | 20.54 | 20.71 | 1.46 | 2.05 | 63.75 | 21.86 | 21.43 | 1.69 | 1.13 |
| FeO | 10.77 | 2.25 | 2.20 | 10.37 | 9.96 | 1.91 | 2.20 | 19.21 | 9.60 | 8.94 | 1.83 | 1.76 |
| MnO | 0.60 | 0.00 | 0.00 | 0.50 | 0.40 | 0.00 | 0.00 | 0.12 | 0.16 | 0.22 | 0.00 | 0.00 |
| MgO | 5.39 | 16.15 | 16.59 | 6.27 | 6.10 | 16.51 | 16.44 | 16.10 | 9.78 | 9.08 | 16.91 | 17.04 |
| CaO | 22.39 | 24.48 | 24.18 | 21.23 | 22.02 | 24.16 | 24.28 | 0.00 | 17.55 | 18.41 | 24.21 | 24.64 |
| $Na_2O$ | 0.00 | 0.76 | 0.89 | 0.00 | 0.00 | 0.90 | 0.74 | 0.00 | 0.00 | 0.00 | 0.62 | 0.42 |
| Total | 100.19 | 100.53 | 99.84 | 98.55 | 99.69 | 101.47 | 101.76 | 99.17 | 100.25 | 99.32 | 101.65 | 101.36 |
| | | | | | | | | | | | | |
| Si | 3.03 | 1.97 | 1.98 | 3.01 | 3.04 | 2.01 | 1.99 | 0.00 | 3.03 | 3.06 | 2.00 | 2.01 |
| Ti | 0.01 | 0.00 | 0.00 | 0.02 | 0.02 | 0.00 | 0.00 | 0.00 | 0.01 | 0.00 | 0.00 | 0.00 |
| Cr | 0.00 | 0.00 | 0.00 | 0.00 | 0.00 | 0.00 | 0.00 | 0.00 | 0.00 | 0.01 | 0.00 | 0.00 |
| Al | 1.85 | 0.10 | 0.06 | 1.85 | 1.84 | 0.06 | 0.09 | 1.97 | 1.90 | 1.88 | 0.07 | 0.05 |
| $Fe^{3+}$ | – | – | – | – | – | – | – | 0.03 | – | – | – | – |
| $Fe^{2+}$ | 0.68 | 0.07 | 0.07 | 0.66 | 0.63 | 0.06 | 0.07 | 0.39 | 0.59 | 0.56 | 0.05 | 0.05 |
| Mn | 0.04 | 0.00 | 0.00 | 0.03 | 0.03 | 0.00 | 0.00 | 0.00 | 0.01 | 0.01 | 0.00 | 0.00 |
| Mg | 0.61 | 0.87 | 0.90 | 0.72 | 0.69 | 0.88 | 0.87 | 0.63 | 1.08 | 1.01 | 0.90 | 0.91 |
| Ca | 1.81 | 0.95 | 0.94 | 1.74 | 1.78 | 0.92 | 0.92 | 0.00 | 1.39 | 1.47 | 0.92 | 0.94 |
| Na | 0.00 | 0.05 | 0.06 | 0.00 | 0.00 | 0.06 | 0.05 | 0.00 | 0.00 | 0.00 | 0.04 | 0.03 |
| Total | 8.03 | 4.01 | 4.02 | 8.04 | 8.02 | 3.99 | 3.99 | 3.02 | 8.01 | 8.00 | 3.99 | 3.98 |

*Table continues*

TABLE 1. *Continued*

| | Clinopyroxenite 4-1 | | | | | | | Zrc | |
|---|---|---|---|---|---|---|---|---|---|
| Mineral | Grt (exs in Cpx) | Grt (mega) | Cpx (inc in mega Grt) | Amp (inc in Grt) | Amp (exs in Cpx) | Amp (rim around Cpx) | Amp (retrograde) | Grt | Cpx |
| $SiO_2$ | 41.14 | 41.58 | 54.62 | 42.26 | 44.27 | 44.34 | 47.94 | 41.06 | 55.36 |
| $TiO_2$ | 0.02 | 0.06 | 0.00 | 0.50 | 0.15 | 0.14 | 0.26 | 0.00 | 0.00 |
| $Cr_2O_3$ | 0.12 | 0.08 | 0.06 | 0.06 | 0.06 | 0.16 | 0.11 | 0.07 | 0.00 |
| $Al_2O_3$ | 22.91 | 22.41 | 1.02 | 15.12 | 13.49 | 13.73 | 10.81 | 21.53 | 2.12 |
| FeO | 10.21 | 11.41 | 1.80 | 4.62 | 4.57 | 4.40 | 8.34 | 11.98 | 2.39 |
| MnO | 0.24 | 0.35 | 0.00 | 0.02 | 0.03 | 0.03 | 0.12 | 0.13 | 0.00 |
| MgO | 14.15 | 14.78 | 17.18 | 17.89 | 18.56 | 18.89 | 15.69 | 6.69 | 15.41 |
| CaO | 11.16 | 9.15 | 24.69 | 12.16 | 12.19 | 12.18 | 12.47 | 18.38 | 22.76 |
| $Na_2O$ | 0.00 | 0.03 | 0.57 | 3.30 | 3.28 | 2.34 | 0.60 | 0.00 | 1.17 |
| Total | 99.95 | 99.85 | 99.95 | 96.47 | 97.37 | 96.97 | 96.49 | 99.84 | 99.21 |
| | | | | | | | | | |
| Si | 3.00 | 3.03 | 1.98 | 6.03 | 6.27 | 6.33 | 6.82 | 3.08 | 2.01 |
| Ti | 0.00 | 0.00 | 0.00 | 0.05 | 0.02 | 0.02 | 0.03 | 0.00 | 0.00 |
| Cr | 0.01 | 0.00 | 0.00 | 0.01 | 0.01 | 0.02 | 0.01 | 0.00 | 0.00 |
| Al | 1.97 | 1.92 | 0.04 | 2.54 | 2.25 | 2.31 | 1.81 | 1.90 | 0.09 |
| $Fe^{3+}$ | | | | 0.54 | 0.43 | | 0.50 | | |
| $Fe^{2+}$ | 0.62 | 0.70 | 0.05 | 0.02 | 0.11 | 0.53 | 0.50 | 0.75 | 0.07 |
| Mn | 0.01 | 0.02 | 0.00 | 0.00 | 0.00 | 0.00 | 0.01 | 0.01 | 0.00 |
| Mg | 1.54 | 1.61 | 0.93 | 3.81 | 3.92 | 4.02 | 3.33 | 0.75 | 0.84 |
| Ca | 0.87 | 0.71 | 0.96 | 1.86 | 1.85 | 1.86 | 1.90 | 1.48 | 0.89 |
| Na | 0.00 | 0.00 | 0.04 | 0.91 | 0.90 | 0.65 | 0.17 | 0.00 | 0.08 |
| Total | 8.01 | 8.00 | 4.01 | 15.77 | 15.75 | 15.74 | 15.07 | 7.97 | 3.98 |

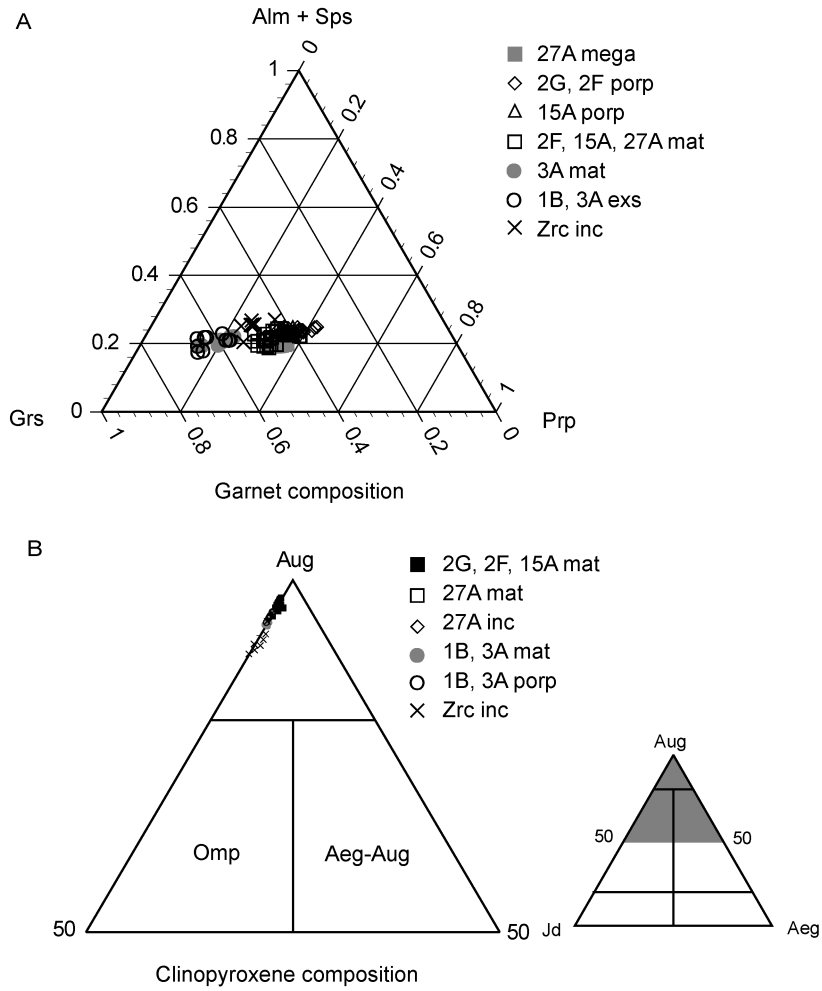


FIG. 6. A. Compositions of megacrystic, porphyroblastic, matrix garnets, garnet exsolutions in porphyroblastic clinopyroxenes, and garnet inclusions in zircons from the Rizhao garnet clinopyroxenites. B. Compositions of porphyroblastic and matrix clinopyroxenes, clinopyroxene inclusions in megacrystic garnet, and clinopyroxene inclusions in zircons from the Rizhao garnet clinopyroxenites. Abbreviations: mega = megacryst; porp = porphyroblast; mat = matrix; exs = exsolution; inc = inclusion.

$Prp_{32.5}Grs_{43.5}Alm_{23.5}Sps_{0.5}$. For porphyroblastic Cpx-bearing clinopyroxenite (type 3), garnet exsolution in cpx porphyroblasts has a similar composition as that of the garnets in matrix. Garnets from type 3 clinopyroxenite are lower in pyrope and higher in grossular contents than those from types 1 and 2 clinopyroxenite. For sample 3A, garnet exsolution in host cpx has an average composition of $Prp_{18.9}Grs_{61.6}Alm_{18.9}Sps_{0.6}$; a garnet rim around a spinel inclusion in coarse-grained cpx shows a composition of $Prp_{19.6}Grs_{62}Alm_{17.9}Sps_{0.5}$; the composition for garnet in the matrix is about $Prp_{19.4}Grs_{60.1}Alm_{19.8}Sps_{0.7}$. For sample 1B, garnet exsolution in cpx has a composition of $Prp_{16.1}Grs_{61.9}Alm_{20.8}Sps_{1.2}$. Garnets from types 1 and 2 clinopyroxenite are characterized by low $TiO_2$ (0–0.16 wt%) and relatively high $Cr_2O_3$ (0–0.56 wt%) contents; garnets from type 3 clinopyroxenite contain higher $TiO_2$ (0.09–0.40 wt%) but very low $Cr_2O_3$ (0–0.02 wt%) contents.

### *Clinopyroxene*

Similar compositions were obtained for exsolution-rich porphyroblastic Cpx, Cpx in the matrix, or

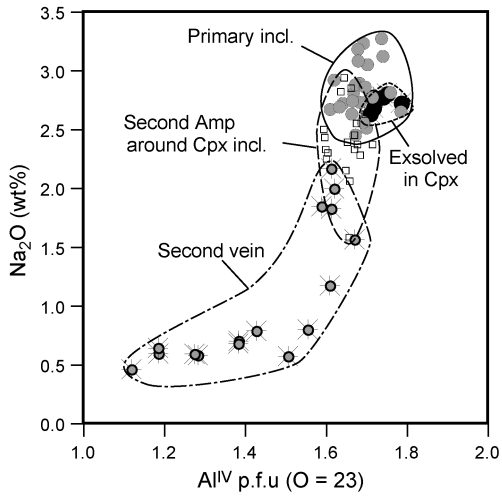


FIG. 7. Compositions of amphiboles as primary inclusions in megacrystic garnet, exsolution in clinopyroxene inclusions in garnet, secondary rims around clinopyroxene inclusions, and secondary vein crosscutting megacrystic garnet.

inclusions in megacrystic garnet. The analyzed clinopyroxenes are diopside with $Jd_{3-8}$ and negligible Aeg component (Fig. 6B). Lamellae-bearing porphyroblastic clinopyroxene has a composition of $Wo_{49.9-50.1}En_{45.9-46.5}Fs_{3.6-4}$, with low FeO (2.17–2.65 wt%) and $Al_2O_3$ (1.97–3.58 wt%). Fine-grained clinopyroxene in the matrix has a composition of $Wo_{48.6-50}En_{47.3-48.1}Fs_{2.7-3.9}$, with $Al_2O_3$ of 0.72–3.57 wt% and FeO of 1.47–2.93 wt%. Clinopyroxene inclusions in megacrystic garnet show a composition of $Wo_{49.4}En_{47.2}Fs_{3.4}$, with similar $Al_2O_3$ (1.69–2.97 wt%) and FeO (1.83–2.28 wt%) content.

*Olivine*

Olivine from the olivine-bearing clinopyroxenite 2G is Mg-rich forsterite and shows distinct compositional zoning (see Fig. 2D), with $Fo_{80-82}$ in the core and $Fo_{75}$ in the rim (Table 1). Most analyzed olivine grains from this sample contain low MnO (0.2–0.4 wt%), CaO (<0.08 wt%), and $TiO_2$ (<0.12 wt%). Olivine from dunite 3B is relatively homogeneous, and is more Mg-rich ($Fo_{92}$) than that from the clinopyroxenite. It also contains low MnO (<0.11 wt%); both CaO and $TiO_2$ contents are below detection limits.

*Amphibole*

Amphibole occurs as primary inclusions in megacrystic garnet, exsolution lamellae in clinopyroxene inclusions, and secondary rims around clinopyroxene inclusions in megacrystic garnet from sample 4-1. These amphiboles are pargasitic hornblende with similar compositions, except that amphibole as primary inclusions has the highest $Na_2O$ content, and secondary amphible around clinopyroxene inclusions has the lowest $Na_2O$ content (Fig. 7). These pargasitic hornblendes contain a considerable amount of $K_2O$ (0.50–1.01 wt%). They are high in $Al_2O_3$ (13–14 wt%) and magnesian (Mg/Mg + $Fe^{2+}$ = 0.87–1.00); these characteristics are similar to those of upper mantle–derived amphiboles (Haggerty, 1995). Amphibole also occurs in a retrograde vein cross-cutting the megacrystic garnet. This secondary amphibole contains lower $Na_2O$ (0.47–2.17 wt%) and $Al^{IV}$ (1.117–1.669) contents. Minor secondary amphibole also occurs in dunite 3B. It is tremolite with a high Mg/(Mg + Fe) of about 0.97.

*Chromite and spinel*

Matrix chromite in dunite 3B contains high $Cr_2O_3$ (50–54 wt%); the Cr/(Cr+Al) ratio is 0.76–0.79, whereas Mg/(Mg + $Fe^{2+}$) is 0.25–0.26. On the other hand, green spinel occurs as both inclusion and matrix phases in clinopyroxenite. In sample 15A, spinel inclusions in garnet porphyroblasts are an Mg-and Al-rich variety; the Cr/(Cr + Al) ratio is 0.05 and the Mg/(Mg + $Fe^{2+}$) ratio is about 0.60. In sample 3A, spinel also occurs as inclusion in a porphyroblastic clinopyroxene and is rimmed by garnet overgrowth. This spinel contains almost no Cr, and the Mg/(Mg + $Fe^{2+}$) ratio is about 0.62. Spinels from the matrix of sample 2G and retrograde veins crosscutting sample 4-1 are also low in Cr/(Cr + Al) (0–0.03) and Mg/(Mg + $Fe^{2+}$) is 0.43–0.54.

## SHRIMP U-Pb Zircon Dating

*Sample descriptions and analytical method*

Zircons from 19 adjacent garnet clinopyroxenite samples from the Hujialing body were dated by SHRIMP. Zircons were separated according to the following procedure. (1) 19 samples of 1–2 kg each were crushed and sieved to small grain size. (2) Hand magnets were used to remove iron fillings and metal oxides from the sample. (3) A slope magnetic separator was then used to separate lower magnetic susceptibility minerals such as zircon and apatite from iron-bearing phases like garnet, olivine, and pyroxene. (4) Apatite was separated from zircon by desilting using alcohol (or by heavy liquid

techniques), and minor metal sulfide was removed by high-frequency dielectric separation. Finally (5) zircons were hand-picked using a binocular microscope.

Zircon separates were mounted in epoxy, polished, and coated with gold before analysis. Cathodoluminescence (CL) examination was done with a JEOL JSM 5600 scanning electron microscope; U-Pb analyses employed the SHRIMP-RG (sensitive high-resolution ion microprobe-reverse geometry) at the Stanford/United States Geological Survey Microanalytical Center. Analytical spots ~30 μm in diameter were sputtered using an ~5 nA $O^{2-}$ primary beam. Six scans through a 9 mass table were made for data collection. The measured $^{206}Pb/^{238}U$ ratios were calibrated with standard zircon R-33 (419 Ma, quartz diorite of Braintree complex, VT; Black et al., 2004), and the U concentrations were calibrated with standard zircon CZ3 (550 ppm U). Data reduction and processing used the SQUID and ISOPLOT (Ludwig, 2001a, 2001b). Isotope ratios and individual ages in Table 2 are reported with 1σ errors, but the weighted mean ages are quoted at 2σ.

## Results

Zircons show rounded to subrounded shape and the size ranges from 60–100 μm. Some zircon grains are homogeneous and exhibit strongly luminescent CL images, whereas others show slightly patchy to chaotic internal structure and are relatively weakly luminescent. Most grains are surrounded by thin, relatively stronger luminescent CL rims (Fig. 8) that are too thin to analyze. Garnet, clinopyroxene, and dolomite inclusions in these zircons were analyzed using a JEOL 733 superprobe at Stanford University. Garnet has a large compositional range ($Prp_{23-30}Grs_{43-54}Alm_{20-27}Sps_{0.2-0.7}$), with low $TiO_2$ (0–0.12 wt%) and $Cr_2O_3$ (0–0.11 wt%). Clinopyroxene ranges from $Jd_5$ to $Jd_{11}$, but with a relatively homogeneous Ca/Mg/Fe ratio (about $Wo_{49.4}En_{47.1}Fs_{3.5}$). $Al_2O_3$ (1.1–2.5 wt%) and FeO (1.8–2.5 wt%) are also low for the clinopyroxenes.

The SHRIMP U-Pb data are summarized in Table 2. Eleven spot analyses were conducted on 11 zircon grains. Our analyses yielded U contents between 34 and 1226 ppm, with most in the range of 100–300 ppm. Th contents range from 16 to 258 ppm and Th/U ratios are from 0.06 to 0.94 (Fig. 9). All analyses plot near the concordia on a Tera-Wasserburg (TW) diagram (Fig. 10). The $^{207}Pb$ corrected $^{206}Pb/^{238}U$ age for each analysis ranges from 209 to

TABLE 2. U-Th-Pb SHRIMP Zircon Data from the Rizhao Garnet Clinopyroxenite (HJL) from the Sulu Terrane[1]

| Spot name | U, ppm | Th, ppm | Th/U | Common $^{206}Pb$, % | Uncorrected $^{238}U/^{206}Pb$ | Uncorrected $^{207}Pb/^{206}Pb$ | $^{206}Pb^*/^{238}U$ | $^{206}Pb^*/^{238}U$ age, Ma |
|---|---|---|---|---|---|---|---|---|
| Garnet clinopyroxenite HJL34 | | | | | | | | |
| HJL-2 | 153 | 139 | 0.94 | 0.13 | 29.2056 ± 0.9698 | .0515 ± 4.5191 | .0342 ± .0003 | 217 ± 2 |
| HJL-5 | 134 | 30 | 0.23 | 0.30 | 30.2841 ± 1.0421 | .0527 ± 4.0453 | .0329 ± .0004 | 209 ± 2 |
| HJL-6 | 1226 | 258 | 0.22 | –0.03 | 29.5188 ± 0.3854 | .0502 ± 1.3379 | .0339 ± .0001 | 215 ± 1 |
| HJL-10 | 223 | 89 | 0.41 | –0.03 | 30.2796 ± 0.7792 | .0500 ± 3.1084 | .0330 ± .0003 | 210 ± 2 |
| HJL-11 | 281 | 16 | 0.06 | 0.04 | 29.6789 ± 0.7343 | .0508 ± 2.9107 | .0337 ± .0003 | 214 ± 2 |
| HJL-15 | 128 | 53 | 0.42 | 0.07 | 30.1549 ± 1.0715 | .0509 ± 4.2947 | .0331 ± .0004 | 210 ± 2 |
| HJL-16 | 128 | 83 | 0.67 | 0.52 | 29.5491 ± 1.0542 | .0545 ± 4.1979 | .0337 ± .0004 | 214 ± 2 |
| HJL-17 | 584 | 94 | 0.17 | 0.06 | 28.9105 ± 0.5009 | .0510 ± 2.0014 | .0346 ± .0002 | 219 ± 1 |
| HJL-18 | 34 | 19 | 0.57 | 0.03 | 29.9952 ± 2.0609 | .0508 ± 8.1927 | .0345 ± .0007 | 219 ± 5 |
| HJL-19 | 202 | 91 | 0.47 | –0.02 | 29.6670 ± 0.8726 | .0503 ± 3.4749 | .0337 ± .0003 | 214 ± 2 |
| HJL-20 | 360 | 46 | 0.13 | 0.18 | 29.3429 ± 0.6733 | .0519 ± 2.5963 | .0340 ± .0002 | 216 ± 2 |

[1]Pb* corrected for common Pb using $^{207}Pb$ (Williams, 1998). All errors are 1σ of standard deviation.

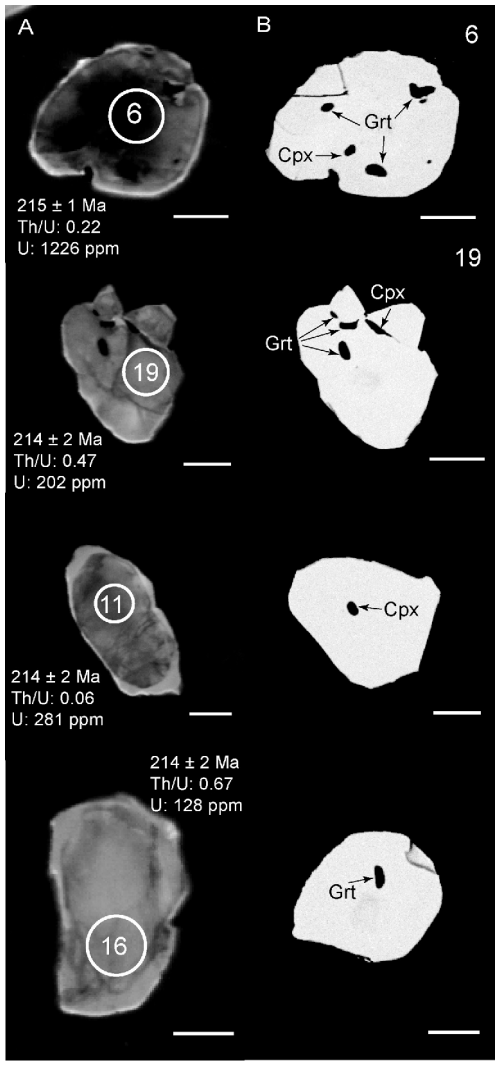


FIG. 8. A. Cathodoluminescence (CL) images of zircons from the Rizhao garnet clinopyroxenite. B. BSE images of zircons from the same sample showing inclusions of garnet and clinopyroxene. Scale bars are 30 μm.

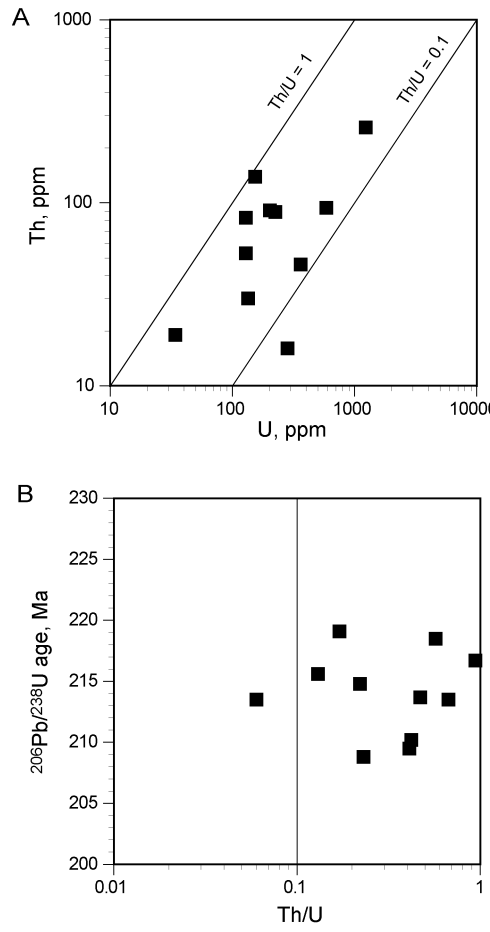


FIG. 9. U and Th concentrations (A), and Th/U ratio versus $^{206}Pb/^{238}U$ age of zircons (B) from the Rizhao garnet clinopyroxenite.

219 Ma; the weighted mean $^{206}Pb/^{238}U$ age is 215 ± 2 Ma ($n$ = 11; MSWD = 3.9).

## Discussion

### *Origin and metamorphic evolution*

The Rizhao garnet clinopyroxenite has been reported to show a mantle signature, such as $^{87}Sr/^{86}Sr$ (0.7038–0.7044), $^{143}Nd/^{144}Nd$ (0.5127–0.5128), and $\delta^{18}O$ in garnet (4.83–5.64‰) and clinopyroxene (4.99–5.64‰) (Jahn, 1998; Zhang et al., 2000). It has the lowest $^{87}Sr/^{86}Sr$ and the highest $^{143}Nd/^{144}Nd$ ratios among all analyzed peridotites from the Sulu terrane (Zhang et al., 2000), which indicates that it may have crystallized in the upper mantle. It shows convex upward REE patterns (Li et al., 1993; Jahn, 1998), which has been found in pyroxenite xenoliths and pyroxenite layers in alpine peridotites (McDonough and Frey, 1989). This may suggest that it is related to the accumulation of clinopyroxene during magma differentiation in the mantle.

The initial tectonic setting and history of the Hujialing clinopyroxenite remain controversial.

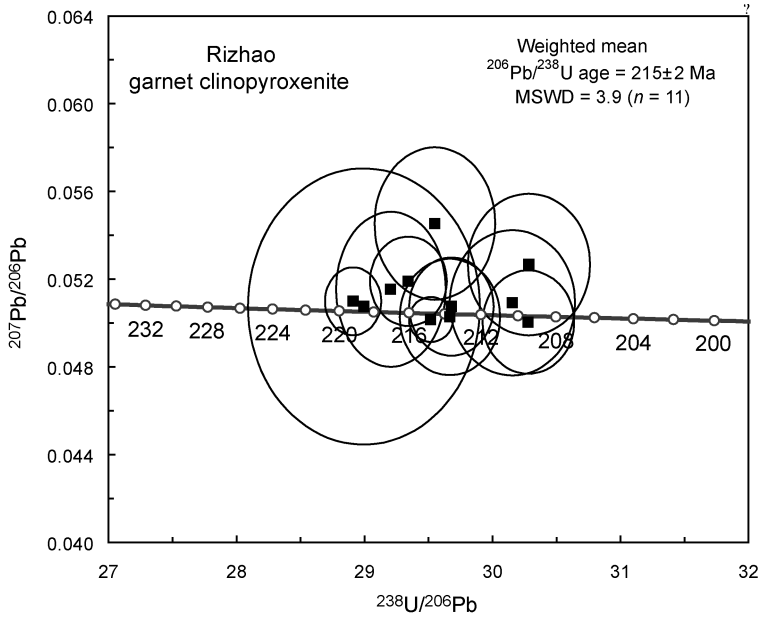


FIG. 10. Tera-Wasserburg diagram showing SHRIMP U-Pb analyses of zircons from the Rizhao garnet clinopyroxenite. Uncorrected ratios are plotted. Error ellipses are shown as 1σ, whereas the uncertainty of the weighted mean age is 2σ. MSWD = mean square of weighted deviates.



Zhang and Liou (2003) studied two representative garnet clinopyroxenites characterized by Grt + Ilm exsolution in the clinopyroxene host. They interpreted the parental phase as either a homogeneous clinopyroxene formed at near-solidus conditions (hypothesis A) or a majoritic garnet from the mantle transition zone at high P (hypothesis B). However, both hypotheses have problems. Hypothesis B cannot explain the occurrence of low-pressure Mg-Al spinel inclusions in both porphyroblastic garnet and lamellae-rich clinopyroxene (which makes hypothesis A more plausible). However, hypothesis A cannot account for the high Ti and $H_2O$ content in the Rizhao clinopyroxenite as indicated by abundant ilmenite and amphibole exsolution in clinopyroxene. Experimental study by Zhang et al. (2003) used Rizhao garnet clinopyroxenite as starting material and showed that the Ti solubility has a pronounced positive correlation with pressure between 5 and 15 GPa in garnet, but is low in coexisting clinopyroxene. Chen and Xu (2005) also suggested a pressure of 8 GPa for the formation of the amphibole-bearing clinopyroxene in order to account for the contained ~2000 ppm $H_2O$.

Here we propose a new hypothesis C modified after hypothesis B of Zhang and Liou (2003). The Rizhao clinopyroxenite is considered to have a five-stage evolution as described below (Figs. 11 and 12).

*Stage I: Formation of spinel clinopyroxenite at shallow depth (1–2 GPa).* We suggest that the protolith of the Hujialing clinopyroxenite body is spinel clinopyroxenite that formed at a shallow depth where Mg-Al spinel was stable. This is supported by spinel inclusions in porphyroblastic garnet from sample 15A (Fig. 2B) and a spinel + ilmenite + magnetite grain enclosed by a thin garnet rim around in a cpx porphyroblast from sample 3A (Fig. 4B). Magnetite and ilmenite also grew together with spinel during this stage, inasmuch as spinel inclusions are invariably associated with these two minerals. Based on the experimentally determined stability field for the spinel peridotite (Gasparik, 1984; Wood and Holloway, 1984; Herzberg and Gasparik, 1991), we assume a pressure of around 1–2 GPa for stage I.

*Stage II: Growth of majoritic garnet at the transition zone (>15 GPa).* After the formation of the spinel clinopyroxenite protolith, the Hujialing body was carried to the great depths (>450 km) by mantle

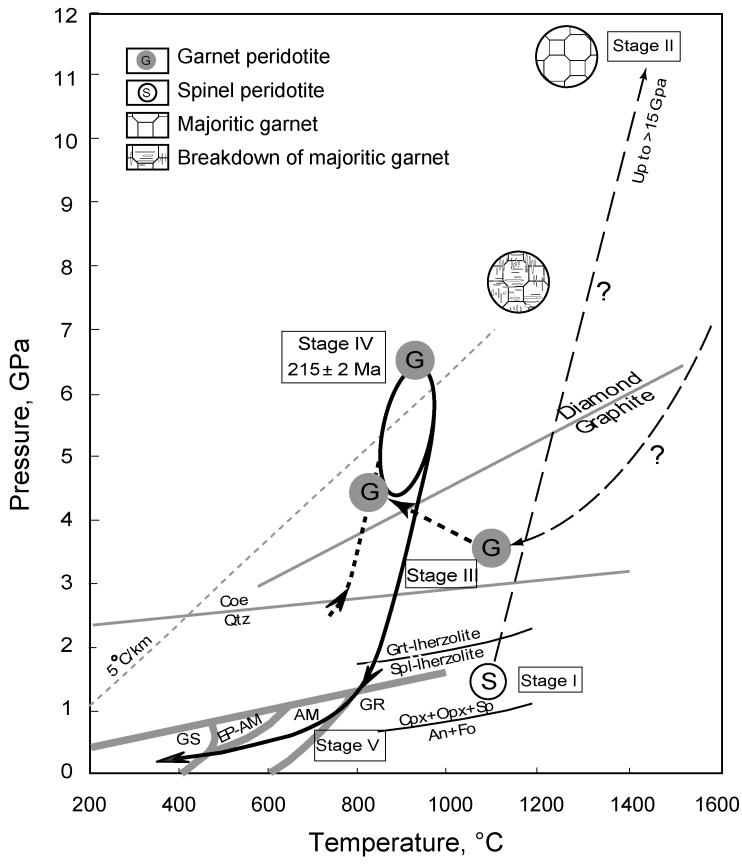


FIG. 11. Reconstructed P-T-time paths of the Rizhao garnet clinopyroxenite. Stage I = original spinel clinopyroxenite; Stage II = formation of majoritic garnets at the mantle transition zone; Stage III = majoritic garnets exsolved to Cpx + Grt + Ilm ± Amp intergrowths during decompression; Stage IV = formation of porphyroblastic /megacrystic garnets and recrystallization of matrix Cpx + Grt + Ilm under UHP conditions; Stage V = retrogression during exhumation.

convection and formed majoritic garnet according to the Zhang et al. hypothesis B. At P > 15 GPa and T = ~1400°C, this majoritic garnet would contain high CaO and considerable amounts of FeO, $TiO_2$, $Na_2O$, and trace $H_2O$ (Zhang and Liou, 2003; Zhang et al., 2003), and thus is qualified as the precursor of the clinopyroxene with Grt + Ilm ± Amp exsolution. Chen and Xu (2005) also suggested a high-pressure (up to 8 GPa) origin for the precursor of lamellae-rich clinopyroxene from this area in order to accommodate a considerable amount of $H_2O$ in Cpx, as indicated by amphibole exsolution.

*Stage III: Exsolution of Cpx + Grt + Ilm ± Amp during decompression (720–880°C, 3 GPa).* Following stage II, the Hujialing body returned to shallow depth through mantle convection, and was emplaced into the subducting slab during the Triassic continental collision. Homogeneous Ti-bearing majoritic garnet broke down to form Cpx + Grt + Ilm ± Amp intergrowth during decompression (Figs. 3–5). Pargasitic amphibole is stable at pressures up to 3.2 GPa at 900°C (Niida and Green, 1999), and thus we assume that the pargasitic amphibole exsolutions appear at P ≤ 3 GPa in the clinopyroxene. Temperatures were estimated using three Fe-Mg exchange geothermometers (Powell, 1985; Krogh, 1988; Ravna, 2000). In this study, all Fe is assumed to be $Fe^{2+}$ for Cpx and Grt. The temperature estimate for this stage is based on garnet exsolution-host clinopyroxene pairs. Sample 1B yields temperatures from 720–850°C, and sample 3A gives a range of 750–880°C at the assumed pressure of 3 GPa (Table 3).

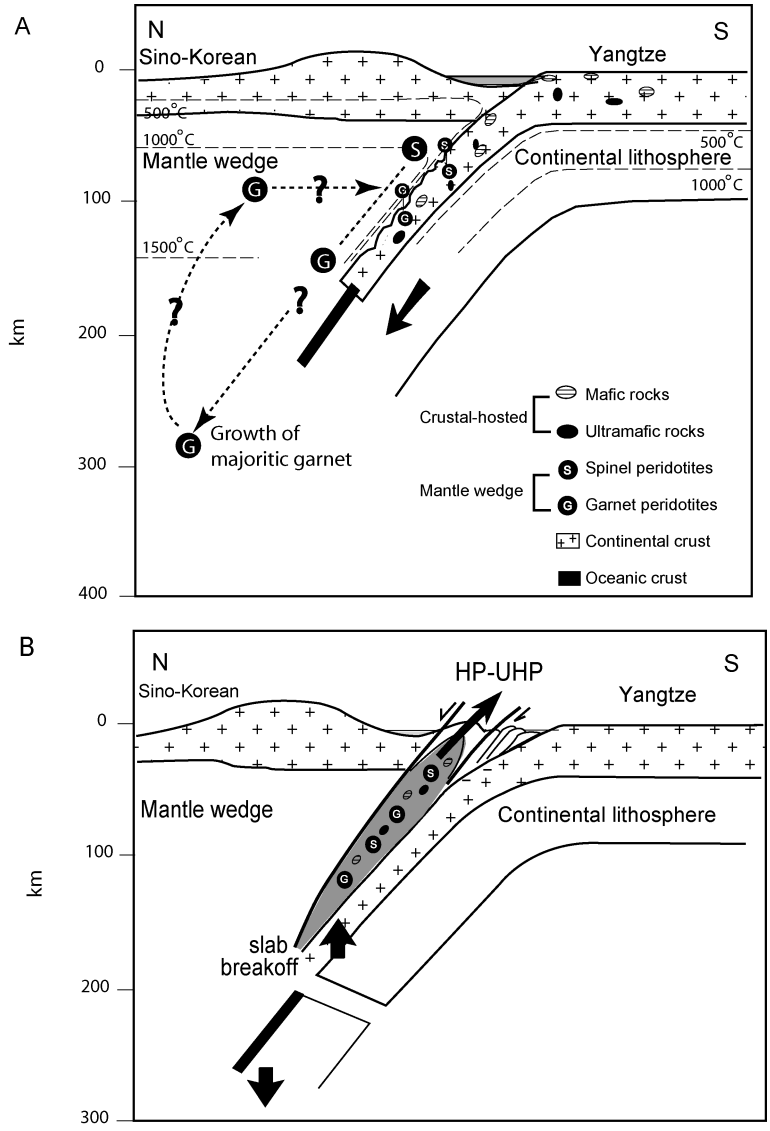


FIG. 12. A tentative model to interpret the origin of the Rizhao garnet clinopyroxenite.

*Stage IV: Growth of porphyroblastic/megacrystic garnet and recrystallization of matrix Cpx + Grt + Ilm under UHP conditions (620–880°C, 3 GPa; 215 Ma).* After emplacement in the subduction zone, the Hujialing body experienced Triassic UHP metamorphism. Porphyroblastic/ megacrystic garnet from types 1 and 2 clinopyroxenite grew during this stage. Garnet coalesced to form megacrysts that engulfed relict lamellae-rich clinopyroxene, ilmenite, and amphibole as inclusions (Fig. 3). Porphyroblastic garnet formed subsequently and lamellae-rich clinopyroxene recrystallized to the matrix assemblage of Cpx + Grt + Ilm. The boundary of clinopyroxene porphyroblasts was obliterated by recrystallization of the matrix minerals as seen in thin section (Fig. 4D).

Quartz pseudomorphs after coesite and abundant exsolved rutile needles are present in garnet from

TABLE 3. P-T Estimates for Different Stages for the Rizhao Garnet Clinopyroxenite

| Type | Sample | | Stage | T °C at P = 30 kbar Grt-Cpx Powell, 1985) | Grt-Cpx (Krogh, 1988) | Grt-Cpx (Ravna, 2000) |
|---|---|---|---|---|---|---|
| 3 | HJL1B | Exs grt - Host cpx | III | 847 | 715 | 727 |
| 3 | HJL3A | Exs grt - Host cpx | III | 883 | 757 | 754 |
| 1 | HJL2G | Mat grt - Mat cpx | IV | 720 | 684 | 616 |
| 1 | HJL2F | Mat grt - Mat cpx | IV | 753 | 716 | 646 |
| 1 | HJL15A | Mat grt - Mat cpx | IV | 816 | 762 | 697 |
| 2 | HJL27A | Mat grt - Mat cpx | IV | 883 | 821 | 754 |
| 3 | HJL3A | Mat grt - Mat cpx | IV | 829 | 717 | 706 |
| | | Zrc Inc. | IV | 839[1] | 769[1] | 733[1] |

[1]Temperature estimates are obtained from mineral inclusions in zircon from the Rizhao clinopyroxenite.



eclogite layers in a nearby ultramafic body (Zhang et al., 2003). This ultramafic has similar rock associations and mineral compositions as the Hujialing body, and may have experienced the same UHP condition during the Triassic subduction (Zhang and Liou, 2003). Therefore, we assume a pressure of ≥3 GPa. Temperature estimates based on matrix Grt–matrix Cpx pairs from type 1 clinopyroxenite (sample 2G, 2F, 15A) yield temperatures from 620–820°C where a pressure of 3 GPa is assumed; in contrast, matrix Grt-Cpx pairs from type 2 (sample 27A) and type 3 (sample 3A) give the temperature range of 750–880°C and 710–830°C, respectively (Table 3). The variation in matrix garnet composition from type 1 and 2 samples to type 3 samples may result from the variation in bulk composition or the slightly different P-T conditions for formation of these garnets.

*Stage V: Retrogression during exhumation.* Many lines of evidence suggest that the Hujialing clinopyroxenite was subjected to retrograde metamorphism during exhumation. Green spinel occurs in the matrix of the clinopyroxenite; a megacrystic garnet was completely replaced by the secondary mineral assemblage Plag + Ep + Chl; another megacrystic garnet is crosscut by a secondary vein consisting of Amp + Spl + Ep + Chl aggregates; matrix garnets are surrounded by a thin kelyphitic corona of epidote, plagioclase, and chlorite. After UHP metamorphism, the Hujialing clinopyroxenite ascended back into the spinel peridotite stability field, and experienced amphibolite- to greenschist-facies retrograde metamorphism at shallower depths. Our speculative hypothesis is basically consistent with the petrographic observations and mineral chemistry, and provides another possible history for the Hujialing garnet clinopyroxenite.

A similar but more complex evolution involving mantle convection has recently been proposed for an orogenic peridotite nodule from the Western Gneiss Region of Norway (Spengler et al., 2006). This Archean Norway mantle peridotite may have been delaminated or sank to the mantle transition zone accompanied by majorite formation, and then became entrained in a subsolidus upwelling followed by emplacement in a Caledonian subduction complex, and exhumation. Moreover, this complex history has been reproduced in numerical studies of early mantle convection (De Smet et al., 2000). However, it deserves further investigation regarding how the Hujialing body traveled from shallow (stage I) to great depths (stage II) in the mantle wedge and back up to shallow depths (stage III) later on, and the emplacement mechanism of the body into the subducting slab. Further detailed experimental and mineralogical studies of the different exsolution features in the porphyroblastic clinopyroxene would be helpful to uncover the P-T-time evolution of the Hujialing clinopyroxenite. The dunite from the Hujialing body may have experienced the same history, but the mineral assemblage (mainly olivine) is too simple to record any such complex P-T evidence. An unserpentinized garnet peridotite from

the Hujialing body might provide important information on its original tectonic setting.

*Formation of zircon and UHPM timing*

Zircons usually do not grow in ultramafic rocks because of the low bulk-rock Zr and Si contents. Zircons in the Hujialing clinopyroxenite may have formed from metasomatic fluid derived either from the subducting slab or from the mantle. Dolomite inclusions were found both in a zircon and a porphyroblastic garnet in the matrix (Fig. 2C). Carbonates (dolomite and magnesite) and hydrous phases (phlogopite and Ti-clinohumite) in peridotite from the CCSD drill hole in conjunction with the formation of zircons have been considered to be the result of metasomatism in the mantle (Zhang et al., 2005a, 2005c). We suggest that the Hujialing clinopyroxenite may have been metasomatized by $CO_2$- and Zr-bearing fluids in the subduction zone. Further REE and stable isotope studies could provide more insights on the nature of the metasomatism.

The morphology, internal structure, and Th-U chemistry of the zircons we studied suggest a metamorphic origin for several reasons. Most zircon grains are equant in shape. Morphology of zircon is considered to be an expression of the stability and the relative growth rates of crystal faces; an isometric/rounded morphology corresponds to the least stability of planar crystal faces and thus the highest metamorphic grade (Vavra et al., 1999). Their homogeneous to patchy CL patterns lack inherited cores, and low Th/U ratios (0.06–0.94) also indicate that these zircons formed during metamorphic recrystallization (Hokada et al., 2004).

Zircon inclusions are present in the matrix clinopyroxene that recrystallized during stage IV; thus we suggest that these zircons have also formed during UHP metamorphism in stage IV. Garnet and clinopyroxene inclusions also occur in zircon (Fig. 8). Compositions of garnet ($Prp_{23-30}Grs_{43-54}Alm_{20-27}Sps_{0.2-0.7}$) inclusions lie between those from type 3 clinopyroxenite (3A, 1B) and the rest of the analyzed garnets (Fig. 6A). Clinopyroxene is relatively rich in Jd component ($Jd_5$ to $Jd_{11}$) and contains less augite content than those matrix and porphyroblastic clinopyroxenes (Fig. 6B). Temperature estimates based on garnet and clinopyroxene inclusions in the same zircon grain are 730–840°C, consistent with estimates for stage IV. The Hujialing body may have been emplaced into the subduction zone (stage III) during its travel from the mantle transition zone (stage II) to shallow depths; the zircons only formed during the later UHP metamorphism (stage IV).

The zircon U-Pb age of 215 ± 2 Ma is slightly younger than the reported UHP ages of 220–240 Ma for the Dabie-Sulu terrane (e.g., Li et al., 1993; Hacker et al., 1998; Liu et al., 2004a, 2004b). However, garnet and clinopyroxene—but no retrograde minerals—are included in zircons from the Rizhao clinopyroxenite. The temperature estimates from these inclusions are within the range of peak metamorphic conditions (750–950°C) for the Dabie-Sulu UHP terrane (Liou and Zhang, 1998; Zhang et al., 2000). This age is not significantly different from eclogites within garnet peridotite from the Rongcheng area which does not show retrograde evidence either (Zhao et al., 2006). Therefore, the 215 ± 2 Ma age is considered as representing the time of UHP metamorphism of the Hujialing ultramafic body.

## Conclusions

Hypothesis C provides an alternative but complicated history for the Rizhao clinopyroxenite, in contrast to hypotheses A and B proposed by Zhang and Liou (2003). The protolith could have been a spinel clinopyroxenite brought to great depths (>450 km) to form majoritic garnet; it then experienced decompression exsolution as it traveled back to shallow mantle depths. During Triassic continental collision, the Rizhao clinopyroxenite body was emplaced into the subduction zone and recrystallized to form megacrystic/porphyroblastic garnet and a matrix assemblage of Cpx + Grt. Our zircon U-Pb dating provides an age constraint of 215 ± 2 Ma for peak UHP metamorphism of the clinopyroxenite body. Hypothesis C still remains to be tested. Systematic experimental and mineralogical investigations are needed to completely understand the evolution history of the Rizhao clinopyroxenite.

## Acknowledgments

We thank J. S. Yang, T. F. Li, S. Z. Chen, and C. L. Wu from Chinese Academy of Geological Sciences for logistical support during our field work. We also thank J. L. Wooden, F. Mazdab, B. Wiegand, and B. Jones for assistance with SHRIMP U-Pb zircon dating, cathodoluminescence imaging, and electron microprobe analyses. We also greatly appreciate critical reviews of the manuscript by Gary Ernst, Michael McWilliams, Page Chamber-

lain, and Norm Sleep. This study was supported in part by NSF EAR 0003355 and EAR 0506901 to J. G. Liou, and by a GSA research grant and Stanford University McGee research grant to R. Zhao.

## REFERENCES

Black, L. P., Kamo, S. L., Allen, C. M., Davis, D. W., Aleinikoff, J. N., Valley, J. W., Mundil, R., Campbell, I. H., Korsch, R. J., Williams, I. S., and Foudoulis, C., 2004, Improved $^{206}Pb/^{238}U$ microprobe geochronology by the monitoring of a trace-element related matrix effect; SHRIMP, ID-TIMS, LA-ICP-MS, and oxygen isotope documentation for a series of zircon standards: Chemical Geology, v. 205, p. 115–140.

Brueckner, H. K., and Medaris, L. G., 1998, A tale of two orogens: The contrasting T-P-t history and geochemical evolution of mantle in high- and ultraigh-pressure metamorphic terranes of the Norwegian Caledonides and the Czech Variscides: Schweizerische Mineralogische und Petrographische Mitteilungen, v. 78, p. 293–307.

Brueckner, H. K., and Medaris, L. G., 2000, A general model for the intrusion and evolution of mantle peridotites in high-pressure and ultrahigh-pressure metamorphic terranes: Journal of Metamorphic Geology, v. 18, p. 123–133.

Chen, J., and Xu, Z. Q., 2005, Pargasite and ilmenite exsolution texture in clinopyroxenes from the Hujialing garnet-pyroxenite, Su-Lu UHP terrane, Central China: A geodynamic implication: European Journal of Mineralogy, v. 17, p. 895–903.

De Smet, J. H., Van den Berg, A. P., and Vlaar, N. J., 2000, Early formation and long-term stability of continents resulting from decompression melting in a convecting mantle: Tectonophysics, v. 322, p. 19–33.

Gasparik, T., 1984, Two-pyroxene thermobarometry with new experimental data in the system CaO-MgO-$Al_2O_3$-$SiO_2$: Contributions to Mineralogy and Petrology, v. 87, p. 87–97.

Hacker, B. R., Ratschbacher, L., Webb, L. E., Ireland, T., Walker, D., and Dong, S., 1998, Zircon ages constrain the architecture of the ultrahigh-pressure Qinling-Dabie orogen, China: Earth and Planetary Science Letters, v. 161, p. 215–230.

Haggerty, S. E., 1995, Upper mantle mineralogy: Journal of Geodynamics, v. 20, p. 331–364.

Herzberg, C., and Gasparik, T., 1991, Garnet and pyroxenes in the mantle: A test of the majorite fractionation hypothesis: Journal of Geophysical Research, v. 96, p. 16,263–16,274.

Hokada, T., Misawa, K., Yokoyama, K., Shiraishi, K., and Yamaguchi, A., 2004, SHRIMP and electron microprobe chronology of UHT metamorphism in the Napier Complex, East Antarctica: Implications for zircon growth at >1,000ºC: Contributions to Mineralogy and Petrology, v. 147, p. 1–20.

Jahn, B.M., 1998, Geochemical and isotopic characteristics of UHP eclogites of the Dabie orogen: Implications for continental subduction and collisional tectonics, *in* Hacker, B., and Liou, J. G., eds., When continents collide: Geodynamics and geochemistry of ultrahigh-pressure rocks: Dordrecht, The Netherlands, Kluwer Academic Publishers, p. 203–240.

Krogh, E. J., 1988, The garnet-clinopyroxene Fe-Mg geothermometer—a reinterpretation of existing experimental data: Contributions to Mineralogy and Petrology, v. 99, p. 44–48.

Li, S., Chen, Y., Cong, B., Zhang, Z., Zhang, R. Y., Liu, D., Hart, S. R., and Ge, N., 1993, Collision of the North China and Yangtze blocks and formation of coesite-bearing eclogite: Timing and processes: Chemical Geology, v. 109, p. 70–89.

Liou, J. G., and Zhang, R. Y., 1998, Petrogenesis of ultrahigh-P garnet-bearing ultramafic body from Maowu, the Dabie Mountains, central China: The Island Arc, v. 7, p. 115–134.

Liu, F., Xu, Z., Liou, J. G., Katayama, I., Masago, H., Maruyama, S., and Yang, J., 2002, Ultrahigh-P mineral inclusions in zircons from gneissic core samples of the Chinese Continental Scientific Drilling Site in eastern China: European Journal of Mineralogy, v. 14, p. 499–512.

Liu F. L., Xu, Z. Q., Liou, J. G., and Song, B., 2004a, SHRIMP U-Pb ages of ultrahigh-pressure and retrograde metamorphism of gneisses, south-western Sulu terrane, eastern China: Journal of Metamorphic Geology, v. 22, p. 315–326.

Liu F. L., Xu, Z. Q., and Xue, H., 2004b, Tracing the protolith, UHP metamorphism, and exhumation ages of orthogneiss from the SW Sulu terrane (eastern China): SHRIMP U-Pb dating of mineral inclusion-bearing zircons: Lithos, v. 78, p. 411–429.

Ludwig, K. R., 2001a, Squid 1.00: A user's manual: Berkeley, CA, Berkeley Geochronology Center, Special Publication, 2, 17 p.

Ludwig, K. R., 2001b, Isoplot/Ex rev. 2.49: A geochronological tool kit for Microsoft Excel: Berkeley CA, Berkeley Geochronology Center, Special Publication 1a, 55 p.

McDonough, W. F., and Frey, F. A., 1989, Rare-earth elements in upper mantle rocks, *in* Lipin, B. R., and McKay, G. A., eds., Geochemistry and mineralogy of rare earth elements: Mineralogical Society of America, Reviews in Mineralogy, v. 21, p. 99–145.

Medaris, L. G., 1999, Garnet peridotites in Eurasian high-pressure and ultrahigh-pressure terranes: A diversity of origins and thermal histories: International Geology Review, v. 41, p. 799–815.

Niida, N., and Green, D. H., 1999, Stability and chemical composition of pargasitic amphibole in MORB pyrolite

under upper mantle conditions: Contributions to Mineralogy and Petrology, v. 135, p. 18–40.

Powell, R., 1985, Regression diagnostic and robust regression in geothermometer/geobarometer calibration: The garnet-clinopyroxene geothermometer revisited: Journal of Metamorphic Geology, v. 3, p. 231–243.

Ravna, E. K., 2000, The garnet-clinopyroxene $Fe^{2+}$-Mg geothermometer: An update calibration: Journal of Metamorphic Geology, v. 18, p. 211–219.

Rumble, D., Giorgis, D., Ireland, T., Zhang, Z., Xu, H., Yui, T. F., Yang, J., Xu, Z., and Liou, J. G., 2002, Low $\delta^{18}O$ zircons, U-Pb dating, and the age of the Qinglongshan oxygen and hydrogen isotope anomaly near Donghai in Jiangsu Province, China: Geochimica et Cosmochimica Acta, v. 66, p. 2299–2306.

Spengler, D., van Roermund, H. L. M., Drury, M. R., Ottolini, L., Mason, P. R. D., and Davies, G. R., 2006, Deep origin and hot melting of an Archaean orogenic peridotite massif in Norway: Nature, v. 440, p. 913–917.

Vavra, G., Schmid, R., and Gebauer, D., 1999, Internal morphology, habit and U-Th-Pb microanalysis of amphibolite-to-granulite facies zircons: Geochronology of the Ivrea Zone (Southern Alps): Contributions to Mineralogy and Petrology, v. 134, p. 380–404.

Williams, I. S., 1998, U-Th-Pb geochronology by ion microprobe, *in* McKibben, M. A., Shanks, W. C., III, and Ridley, W. I., eds., Reviews in Economic Geology, v. 7: Applications of microanalytical techniques to understanding mineralizing processes: Littleton, CO, Society of Economic Geologists, p. 1–35.

Wood, B. J., and Holloway, J. R., 1984, A thermodynamic model for subsolidus equilibria in the system CaO-MgO-$Al_2O_3$-$SiO_2$: Geochimica et Cosmochimica Acta, v. 48, p. 159–176.

Yang, J. J., and Jahn, B.-M., 2000, Deep subduction of mantle-derived garnet peridotites from the Sulu UHPM terrane in China: Journal of Metamorphic Geology, v. 18, p. 167–180.

Yang, J. S., Wooden, J. L., Wu, C. L., Liu, F. L., Xu, Z. Q., Shi, R. D., Katayama, I., Liou, J. G., and Maruyama, S., 2003, SHRIMP U-Pb dating of coesite-bearing zircon from the ultrahigh-pressure metamorphic rocks, Sulu terrane, East China: Journal of Metamorphic Geology, v. 21, p. 551–560.

Ye, K., Yao, Y., Katayama, I., Cong, B. L., Wang, Q. C., and Maruyama, S., 2000, Large areal extent of ultrahigh-pressure metamorphism in the Sulu ultrahigh-pressure terrane of East China: New implications from coesite and omphacite inclusions in zircon of granitic gneiss: Lithos, v. 52, p. 157–164.

Zhang, R. Y., Hirajima, T., Banno, S., Cong, B. L., and Liou, J. G., 1995, Petrology of ultrahigh-pressure rocks from the southern Su-Lu region, eastern China: Journal of Metamorphic Geology, v. 13, p. 659–675.

Zhang, R. Y., and Liou, J. G., 1998, Ultrahigh-pressure metamorphism of the Sulu terrane, eastern China: A prospective view: Continental Dynamics, v. 3, p. 32–53.

Zhang, R.Y., and Liou, J. G., 2003, Clinopyroxenite from the Sulu ultrahigh-pressure terrane, eastern China: Origin and evolution of garnet exsolution in clinopyroxene: American Mineralogist, v. 88, p. 1591–1600.

Zhang, R. Y., Liou, J. G., and Cong, B., 1994, Petrogenesis of garnet-bearing ultramafic rocks and their associated eclogites in the Su-Lu ultrahigh-P metamorphic terrane: Journal of Metamorphic Geology, v. 12, p. 169–186.

Zhang, R. Y., Liou, J. G., Yang, J. S., Li, T. F., Yui, Z., and Li, L., 2005a, Hydrous phase and carbonate-bearing peridotites from the Sulu UHP terrane, China: An excellent record of mantle metasomatism and subduction zone UHP metamorphism [abs.]: EOS (Transactions of the American Geophysical Union, v. 86, no. 52 (Fall Meeting supplement), abstract V53E-08.

Zhang, R. Y., Liou, J. G., Yang, J. S., and Yui, T. F., 2000, Petrochemical constraints for dual origin of garnet peridotites from the Dabie-Sulu UHP terrane, eastern-central China: Journal of Metamorphic Geology, v. 18, p. 149–166.

Zhang, R. Y., Liou, J. G., Zheng, J. P., Griffin, W. L., Yui, T. F., and O'Reilly, S. Y., 2005b, Petrogenesis of the Yangkou layered garnet-peridotite complex, Sulu UHP terrane, China: American Mineralogist, v. 90, p. 801–813.

Zhang, R. Y., Yang, J. S., Wooden, J. L., Liou, J. G., and Li, T. F., 2005c, U-Pb SHRIMP geochronology of zircon in garnet peridotite from the Sulu UHP terrane, China: Implications for mantle metasomatism and subduction-zone UHP metamorphism: Earth and Planetary Science Letters, v. 237, p. 729–743.

Zhang, R. Y., Zhai, S. M., Fei, Y. W., and Liou, J. G., 2003, Titanium solubility in coexisting garnet and clinopyroxene at very high pressure: The significance of exsolved rutile in garnet: Earth and Planetary Science Letters, v. 216, p. 591–601.

Zhao, R., Liou, J. G., Zhang, R. Y., and Li, T., 2006, SHRIMP U-Pb zircon dating of the Rongcheng eclogite and associated peridotite: New constraints for ultrahigh-pressure metamorphism of mantle-derived mafic-ultramafic bodies from the Sulu terrane, *in* Hacker, B. R., McClelland, W. C., and Liou, J. G., eds., Ultrahigh-pressure metamorphism: Deep continental subduction: Geological Society of America Special Paper 403, p. 115–125.